MTLA 28 (2023) 101744

Contents lists available at ScienceDirect

Materialia

journal homepage: www.elsevier.com/locate/mtla

Full Length Article

A simple phenomenological model to describe stability of homogeneous solid solutions in high entropy alloys from metallic bonding potential

J.S. Blázquez *, N. García-Pinto, C.F. Conde

Dpto. Física de la Materia Condensada, ICMSE-CSIC Universidad de Sevilla, P.O. Box 1065, Sevilla 41080, Spain

ARTICLE INFO

Keywords:
High entropy alloys
Metallic bonding
Solid solutions

ABSTRACT

A simple model based on the potential parameters used to describe metallic bonding is extended to solid solutions. A figure of merit (an effective temperature, T_{eff}) is proposed using a simple average over the potential coefficients to discern whether a homogeneous solid solution is expected to be stable or not in high entropy alloy compositions. T_{eff} is calculated as the ratio between the solid solution excess in bonding energy over the average mixture divided by the configurational entropy. Application to the sexinary AlCrCuFeNiCo system stablishes a stability threshold for $T_{eff} < 500$ K. The model can successfully describe both the deviations from Vegard's law observed in binary alloys and the differences in this parameter between B2 ordered and bcc disordered phases considering average potential coefficients over the different possible atomic couples.

Compositional tuning needed to optimize the feasibility, stability, microstructure, phase transitions and functional properties of new alloys generally yields multicomponent alloys (MCAs) with four or more elements [1]. This line of research led to the discovery and development of the so-called high entropy alloys (HEA) proposed by Cantor [2] and Yeh et al. [3] in 2004. These HEA systems are MCAs with close to equiatomic compositions with enhanced configurational entropy. This configurational entropy, ΔS_{conf}, is expected to facilitate the formation of simple metallic phases (monoatomic bcc, fcc and hcp structures, or even amorphous systems) [4–6].

The interest in HEA opened a vast compositional range for alloy design, which phase diagram extension is huge in comparison with those corresponding to the conventional explored regions (close to corners and edges of the multicomponent phase diagrams). In order to clarify this vast compositional region, simulations and theoretical studies [7–11] are very useful to optimize the experimental research time, and helped to point for the most interesting regions of the vast phase diagram depending on the property or functionality of interest. Citing the words of D. B. Miracle (2019) "…*exploring the enormous number of HEA and CCA [complex, concentrated alloys] compositions and their microstructures is currently the biggest challenge.*" [12]. This author poses the development of HEA as a new reinforcement in the alloys design activity but shows the tremendous effort needed to explore the compositional range.

Despite the accepted main role of ΔS_{conf}, this is not the only parameter to consider for single phase formation in MCAs. The present situation is still far from being clear [4,13], although several phenomenological rules have been proposed. These rules are based on different parameters such as mixing enthalpy [8,9,14], valence electron concentration [15], size factor [16,17] and structural misfit [18]. These parameters are generally based on reasoning followed to understand binary alloys [14,15,19] and summarized in the empirical Hume-Rothery's rules [20] and semiempirical Miedema's model [21]. More recently, King et al. [19,22] have developed a software (Alloy Search and Predict, ASAP [23]) for a rapid estimation of the single phase HEA systems based on the Miedema's values of enthalpy of mixing. In these papers the authors define a parameter $\phi = -\Delta G_{ss}/|\Delta G_{max}|$, where ΔG_{ss} is the Gibbs free energy for the solid solution and ΔG_{max} is the extreme value of any binary system among the constituents (negative and minimum for intermetallic, positive and maximum for segregation). The use of the absolute value considers both destabilization ways of the solid solution: the affinity to form an intermetallic phase as well as the positive enthalpy of mixing between the elements leading to segregation. King et al. [19] proposed a value of $\phi \geq 1$ as indicative of stable solid solution. On the other hand, Gorban et al. [15] proposed the electron concentration per atom, C_{sd}, as the main factor to classify the microstructures of HEA compositions: bcc solid solution ($4.2 < C_{sd} < 7.2$), fcc solid solution ($C_{sd} \geq 7.5$), two-phase solid solutions ($7.2 < C_{sd} < 8.0$), Laves phase ($4.4 < C_{sd} < 8.1$), σ phase ($6.3 < C_{sd} < 7.2$), μ phase ($C_{sd} \sim 7.3$).

* Corresponding author.
E-mail address: jsebas@us.es (J.S. Blázquez).

https://doi.org/10.1016/j.mtla.2023.101744
Received 30 November 2022; Accepted 11 March 2023
Available online 14 March 2023

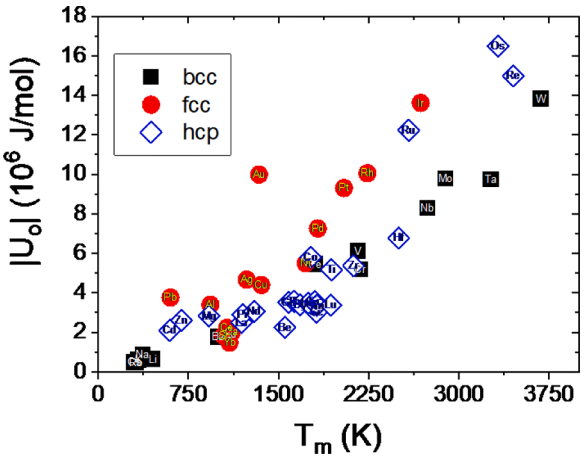

Fig. 1. Estimated bonding energy from Eq. (3) as a function of melting temperature for different pure metals as a function of their crystalline structure.

In this work, we develop a simple model from the potential energy for metallic bonding and extend it to alloys by assuming a near neighbors approximation. The proposed approach is able to describe the deviation of lattice parameter from linearity of Vegard's law as well as the differences between ordered and disordered phases. Moreover, a figure of merit is proposed as an effective temperature that can distinguish between HEA compositions leading to multiphase systems or single phase ones.

Atomic bonding in solids is described taking into account two contributions to the cohesion energy: an attractive term and a repulsive one. In the case of metallic bonding, the attractive term is due to the interaction between the electron cloud dispersed in the solid and the lattice ions whereas the repulsive term is due to the increase in the energy of the fermionic electron cloud when its volume is reduced (see Supplemental content). This leads to the following general expression for the cohesion energy per atom [24]:

$$\frac{U}{N} = -\frac{A}{r} + \frac{B}{r^2} \tag{1}$$

where A and B are parameters of the solid and r is the distance between first neighbors. In order to obtain those two parameters for each metal, we can use the experimental values of the lattice parameter, a, and the compressibility, κ. The former is related to the equilibrium distance between first neighbors ($dU/dr|_{r_0} = 0$):

$$r_0 = \frac{2B}{A} = \alpha a \tag{2}$$

Where $\alpha = \sqrt{3}/2$ for monoatomic body centered cubic (bcc), $1/\sqrt{2}$ for monoatomic face centered cubic (fcc), and 1 for hexagonal close packed (hcp) structures (for simplification we have assumed perfect hcp structures). Therefore, the cohesion energy per atom in a pure metal at equilibrium distance is:

$$\frac{U_0}{N} = -\frac{A^2}{4B} \tag{3}$$

The inverse of the compressibility (bulk modulus) is related to the second derivative of the cohesion energy:

$$\frac{1}{\kappa} = -V\frac{dP}{dV}\bigg|_{eq} = N^2\beta r_0^3\left(-\frac{2A}{r_0^3} + \frac{6B}{r_0^4}\right)\left(\frac{1}{3N\beta r_0^2}\right)^2 = \frac{1}{144\beta}\frac{A^5}{B^4} \tag{4}$$

Where the volume of the solid has been used: $V = N\beta r^3$, with $\beta = 4/\sqrt{27}$ for bcc and $\beta = 1/\sqrt{2}$ for fcc and hcp. Taking into account Eqs. (2) and

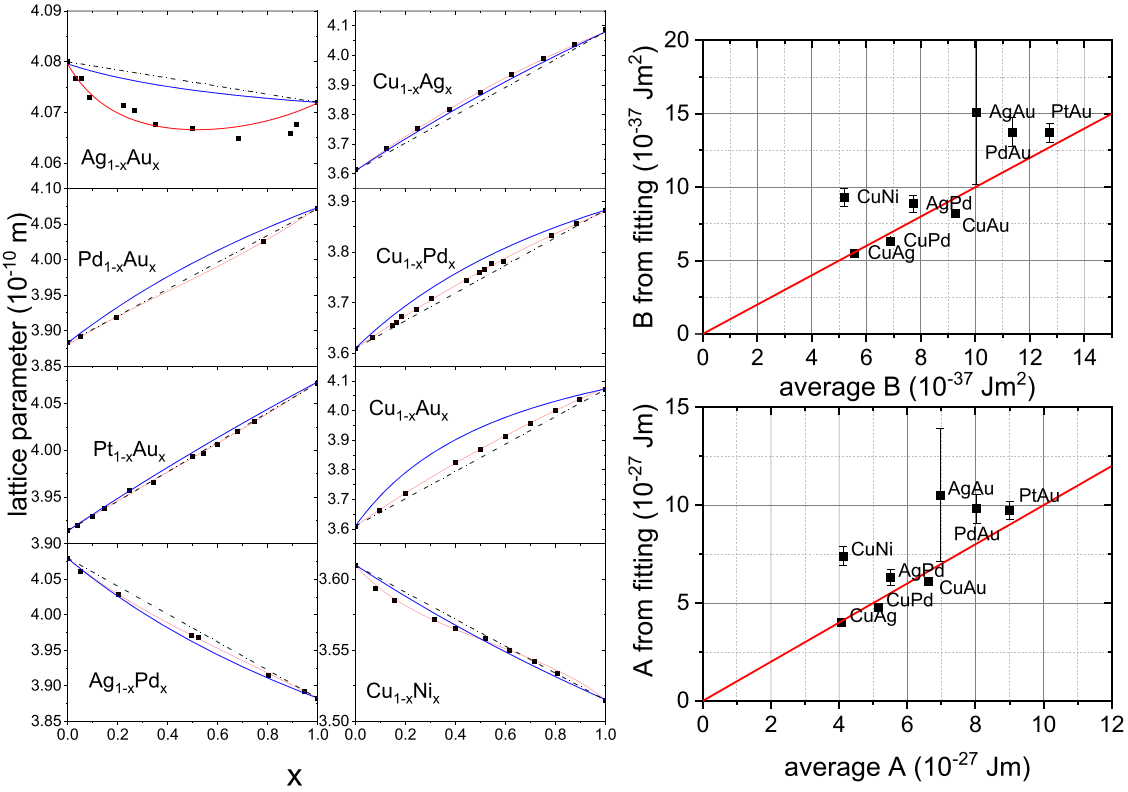

Fig. 2. (left panels) Lattice parameter as a function of the composition for different binary solid solutions. Data taken from [26] are plotted as squares; broken lines correspond to Vegard's law; blue lines correspond to average model using $\langle A\rangle = xA_{M1} + (1-x)A_{M2}$ and $\langle B\rangle = xB_{M1} + (1-x)B_{M2}$; red lines correspond to using Eq. (8) taking A_{Mi} and B_{Mi} from Table 1S (supplemental content) and fitting A_{M12} and B_{M12}. (Right panels) Fitted A_{M12} and B_{M12} parameters vs. corresponding average values $\langle A\rangle = xA_{M1} + (1-x)A_{M2}$ and $\langle B\rangle = xB_{M1} + (1-x)B_{M2}$. Red lines correspond to the identity $A_{M12} = \langle A\rangle$ and $B_{M12} = \langle B\rangle$.

(4), it is possible to obtain the values of A and B for each metal from the experimental values of a and $1/\kappa$ as:

$$A = 9\beta\alpha^4\frac{a^4}{\kappa} \tag{5}$$

and

$$B = \frac{9}{2}\beta\alpha^5\frac{a^5}{\kappa} \tag{6}$$

Table 1S (Supplemental content) collects the lattice parameter (taken from [25,26]), bulk modulus [27] and A and B parameters for different pure metals crystallizing in bcc, fcc, hcp or double hcp (Dhcp) structures. In the Supplemental content, simple models for A and B are described to associate them with the valence electrons, as estimated by Pauling [28] (See Fig. 1S in Supplemental content).

From the data of Table 1S and using Eq. (3) it is possible to estimate the equilibrium energy of the bonding, U_0. Fig. 1 shows the absolute value of this energy per mol as a function of the melting temperature, T_m, for the different metallic elements grouped by their crystalline structures. A general linear trend is observed validating the potential used to describe the metallic bonding.

Eq. (2) relates the lattice parameter with the bonding coefficients A and B in pure metals. This can be extended to binary systems assuming average values of these interaction coefficients. Considering that interactions are finally ascribed to couples of atoms, we can approach the average value of bonding coefficients from averaging the possible pairs of atoms, for a solid solution $M1_xM2_{1-x}$, with x the atomic fraction:

$$\begin{aligned}\langle A\rangle &= x^2A_{M1} + 2x(1-x)A_{M12} + (1-x)^2A_{M2}\\ \langle B\rangle &= x^2B_{M1} + 2x(1-x)B_{M12} + (1-x)^2B_{M2}\end{aligned} \tag{7}$$

Where A_{Mi} and B_{Mi} are the corresponding coefficients of the pure Mi metal. Expressions reduce to $\langle A\rangle = xA_{M1} + (1-x)A_{M2}$ and $\langle B\rangle = xB_{M1} + (1-x)B_{M2}$ when $A_{M12} = \frac{1}{2}(A_{M1} + A_{M2})$ and $B_{M12} = \frac{1}{2}(B_{M1} + B_{M2})$, respectively.

Therefore, under this approach, the lattice parameter of a solid solution is predicted to be:

$$a(x) = \frac{2\langle B\rangle}{\alpha\langle A\rangle} = \frac{2\left(x^2B_{M1} + 2x(1-x)B_{M12} + (1-x)^2B_{M2}\right)}{\alpha\left(x^2A_{M1} + 2x(1-x)A_{M12} + (1-x)^2A_{M2}\right)} \tag{8}$$

Leading to a nonlinear relationship between the lattice parameter and the atomic fraction unlike the linear one predicted by Vegard's law which is based on the hard spheres approximation. The approximate character of Vegard's law [29] is long time known [30] and independent of the metallic bonding character. In fact, deviations from Vegard's law are also reported for covalent [31,32] and ionic [33,34] bonding. Friedel [30] ascribed these deviations in binary solid solutions to the difference in the compressibility of the pure elements. Magadenov [35] recently proposed a method for obtaining lattice parameter of binary alloys at different pressures taking into account the differences in compressibility and specific volume between pure systems. However, in general, continuum elasticity models [36] do not correctly predict the deviations found due to the atomistic character of the problem [37]. King [38] proposed that deviations from Vegard's law are indicative of electron transfer between the constituent atoms leading to changes in their effective radii.

Lattice parameter of several binary solid solutions (data taken from [26]) were fitted to Eq. (8) and shown in Fig. 2. This figure also shows the Vegard's law (dashed lines) and the non-free parameter curves obtained using $A_{M12} = \frac{1}{2}(A_{M1} + A_{M2})$ and $B_{M12} = \frac{1}{2}(B_{M1} + B_{M2})$ (blue curves); in the following named as average model. In general, it is worth mentioning that non-free parameter curves correctly predict the sense of deviation of the data from Vegard's law. Concerning the magnitude of the deviation, this can be overestimated (e.g. Pd-Au) or underestimated (e.g. Ag-Au). The particular case of Ag-Au system is indicative of the limitations of the average model as it cannot predict intermediate

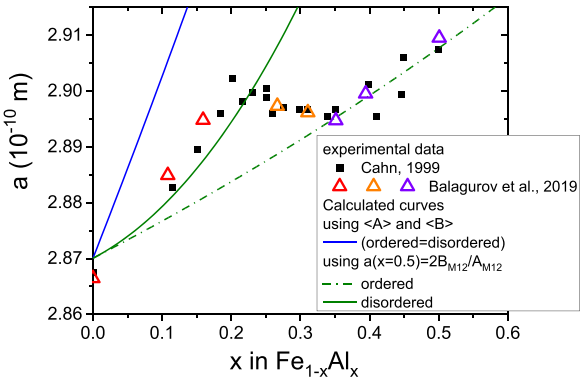

Fig. 3. Lattice parameter of ordered and disordered $Fe_{1-x}Al_x$ alloys. Experimental data taken from [41] (black squares) and [40] (hollow triangles: red corresponds to disordered bcc, orange to half lattice parameter of ordered DO_3 phase, and purple to ordered B2 phase). Blue line corresponds to the calculated curve using $A_{M12} = (A_{Al} + A_{Fe})/2$ and $B_{M12} = (B_{Al} + B_{Fe})/2$ and predicted lattice parameters for ordered and disordered phases are indistinguishable. Green curves correspond to calculated curves taken $r_{BA} = B_{M12}/A_{M12} = \left(\frac{\sqrt{3}}{4}\right)a(x = 0.5)$. Maximum ordered (dash-dotted lines) and fully disordered (solid lines) phases are now distinguishable.

compositions beyond the lattice parameters of both pure metals. However, deviations from the average model in most cases are not as high as left panels of Fig. 2 suggest. In fact, it must be taken into account that the parameters used derive from experimental data of lattice parameter and bulk modulus of pure metals. Particularly, the latter presents large errors [27]. Fig. 2 also shows the comparison between fitted A_{M12} and B_{M12} parameters and the corresponding average values $\langle A\rangle = xA_{M1} + (1-x)A_{M2}$ and $\langle B\rangle = xB_{M1} + (1-x)B_{M2}$. Values are generally close to the identity line. However, Ag-Au and Cu-Ni systems clearly deviate. In fact, average model would not be able to explain differences in the lattice parameter between ordered and disordered phases. However, although limited to first neighbors, the proposed model can explain why lattice parameter differs between ordered and disordered phases, considering that A_{M12} and B_{M12} are not necessarily equal to $\langle A\rangle$ and $\langle B\rangle$, respectively.

In the case of Fe(Al), ordered B2 phase appears in the compositional range from 22 to 54 at.% Al for temperatures above 660 C and below 550 C a DO_3 structure appears [39] in a compositional range from 23 to 31 at.% [40]. Fig. 3 shows the value for the lattice parameter of $Fe_{1-x}Al_x$ alloys for B2 ordered and bcc disordered phases (data taken from [40,41]). When average values for A_{M12} and B_{M12} parameters are considered, no change between the lattice parameter of ordered and disordered phases is predicted (blue line in Fig. 3). In order to obtain the potential coefficients, $B_{M12}/A_{M12} = r_{BA}$ ratio is taken from the experimental value of the lattice parameter of $Fe_{0.5}Al_{0.5}$ alloy, using Eq. (2) and considering a perfect order for this stoichiometric composition. To obtain individual values for A_{M12} and B_{M12}, we took two choices: as a first choice we use the average value for $A_{M12} = (A_{Fe} + A_{Al})/2$ and then calculate $B_{M12} = r_{BA}A_{M12}$. Analogously, a second choice was using $B_{M12} = (B_{Fe} + B_{Al})/2$ and calculate $A_{M12} = B_{M12}/r_{BA}$. Curves can be now calculated assuming perfect disorder (continuous lines) and maximum order (dash-dotted lines), i.e. Al is always in correct positions and Fe excess is placed in Al sites. No significant differences are found whether the first or second choice is taken. Despite the expected errors in lattice parameter, the curves agree with the experimental data in the range of stability of disordered bcc and ordered B2, whereas between $0.22 < x < 0.35$, in the range of DO_3 ordered structure (where half the lattice parameter of the fcc phase is shown [40]), the lattice parameter is almost constant. However, the model, using just first neighbors approach, is not expected to represent this more complex system.

In the frame of the proposed model, it is possible to discuss on the

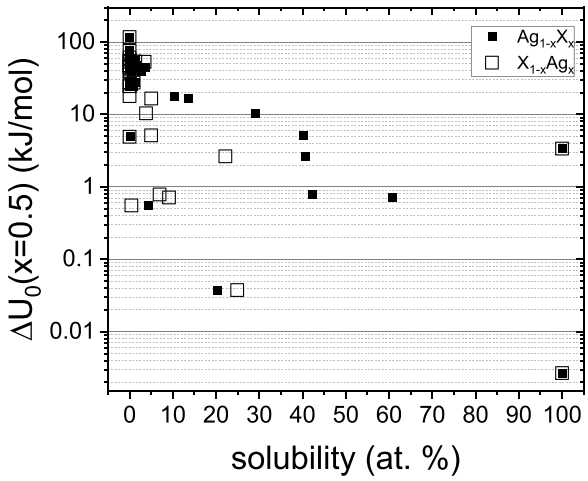

Fig. 4. Differences between the equilibrium energy of an equiatomic supersaturated solid solution and that corresponding to the average of the pure metals for different binary alloys with silver as a function of the maximum solubility (taken from [39]) of the element in Ag fcc phase and vice versa.

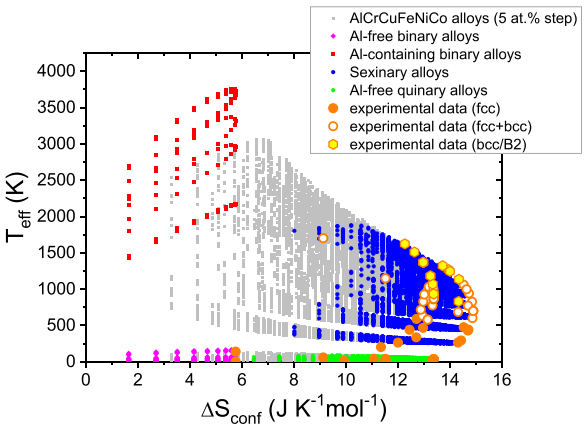

Fig. 5. T_{eff} for 53,130 $Al_{x1}Cr_{x2}Cu_{x3}Fe_{x4}Ni_{x5}Co_{100-\Sigma xi}$ compositions with increments of $\Delta x_i = 5$ at.%. Binary alloys (red symbols) as well as sexinary alloys (blue circles) and Al-free quinary alloys (green circles) are distinguished in the figure. T_{eff} for 70 alloys from literature [42–58] are shown as large orange circles for single phase systems (solid symbols) and multiphase systems: fcc+bcc (hollow symbols) and bcc+B2 (yellow filled symbols).

stability of solid solutions. In fact, using Eq. (3), we can calculate the difference between the energy of an equiatomic solid solution and that of the corresponding mixture of pure components as:

$$\frac{\Delta U_0}{N} = -\frac{\langle A\rangle^2}{4\langle B\rangle} - \frac{1}{2}\left(-\frac{A_{M1}^2}{4B_{M1}} - \frac{A_{M2}^2}{4B_{M2}}\right) = -\frac{(A_{M1}+A_{M2})^2}{8(B_{M1}+B_{M2})} - \frac{1}{2}\left(-\frac{A_{M1}^2}{4B_{M1}} - \frac{A_{M2}^2}{4B_{M2}}\right) \quad (9)$$

Fig. 4 shows the calculated $\Delta U_0/N$ values using data from Table 1S as a function of the maximum solubility (taken from [39]) of different elements in Ag and vice versa. In the average model, calculated values are always positive as Eq. (9) can be written as:

$$\frac{\Delta U_0}{N} = \frac{1}{8}\frac{(A_{M1}B_{M2} - A_{M2}B_{M1})^2}{B_{M1}B_{M2}(B_{M1}+B_{M2})} > 0 \quad (10)$$

However, configurational entropy should lead to stable solid solutions when available. As a general rule, solubility increases as ΔU_0 decreases and $\Delta U_0 > 20\ kJ/mol$ can be used as a rule of thumb to predict insolubility between different elements.

All these features pose a very simple way to predict stability for solid solutions, which can be straightforwardly extended to more complex systems such as HEAs. Once composition is known, ΔS_{conf} (per mol) can be calculated as:

$$\Delta S_{conf} = -R\sum_i x_i log(x_i) \quad (11)$$

Where R is the gas constant and x_i is the atomic concentration of element i with $\sum_i x_i = 1$. Thus ΔS_{conf} is enhanced in equiatomic systems and furthermore by addition of new elements. However, this does not necessarily lead to single phase systems. In fact, whereas $CrCuFeNi_2$ shows a single fcc phase, addition of Al in $Al_xCrCuFeNi_2$ ($0.8<x<1.5$) leads to the formation of fcc and bcc phases [42], despite ΔS_{conf} is enhanced almost 20%. In the frame of the model described here, we can calculate the energy difference per mol between the average over those of pure element phases and the corresponding complete solid solution by extending Eq. (9) to p number of elements:

$$\frac{\Delta U_0}{N_A} = -\frac{\langle A\rangle^2}{4\langle B\rangle} + \sum_i^p x_i\frac{A_{Mi}^2}{4B_{Mi}} \quad (12)$$

Applying this to the previous case, ΔU_0 increases from 0.6 kJ/mol for $CrCuFeNi_2$ system to 13 kJ/mol for $Al_{1.5}CrCuFeNi_2$. The relative change in ΔU_0 clearly exceeds that of ΔS_{conf} and can explain why a single solid solution is not formed for the Al containing composition but the elements partition among three different solid solutions (a bcc and two fcc phases [42]). Energy dispersive X-ray analysis can be found in the literature showing Cu-rich composition for the fcc phases and Fe-rich for the bcc one [42–44]. However, the semiquantitative character of this technique prevents the use of the reported composition data to appreciate a decrease in the relative effect of ΔU_0 and ΔS_{conf}. This can be parametrized in the figure of merit $T_{eff} = \Delta U_0/\Delta S_{conf}$, which is an effective temperature at which excess energy and thermal contribution of configurational entropy compensate each other. Singh et al. [45] applied 3D atom probe analysis (compositional probe within atomic scale) to AlCrCuFeCoNiCo equiatomic alloy and reported the presence of 40 nm sized regions with $Al_3Cr_{40}Cu_1Fe_{31}Ni_6Co_{19}$ composition. The average equiatomic composition should lead to $\Delta U_0 = 10$ kJ/mol and $\Delta S_{conf} = 14.9$ J/molK, whereas in the nanometric regions the corresponding values are $\Delta U_0 = 2.3$ kJ/mol and $\Delta S_{conf} = 11.4$ J/molK. Therefore, T_{eff} reduces from 670 K in the average composition to 200 K in the nanocrystalline phase.

In order to supply a more complete view, Fig. 5 shows T_{eff} values for the 53,130 compositions $Al_{x1}Cr_{x2}Cu_{x3}Fe_{x4}Ni_{x5}Co_{100-\Sigma xi}$ (stepped by $\Delta x_i = 5$ at.%). Al-free and Al-containing binary alloys as well as sexinary alloys and Al-free quinary alloys are distinguished in the figure. The plot exemplifies the formidable problem to be solved when exploring the field for HEA compositions. It can be observed that the presence of Al in sexinary compositions increases T_{eff} with respect to Al-free quinary alloys, explaining why destabilization of single phase solid solutions occurs as it is experimentally observed.

Experimental data on $Al_{x1}Cr_{x2}Cu_{x3}Fe_{x4}Ni_{x5}Co_{100-\Sigma xi}$ compositions (70 alloys with around 50 different compositions taken from [42–58]) are also shown in Fig. 5. In this figure, it is indicated whether the alloy appears as a single fcc solid solution (solid orange circles), as bcc plus B2 phases (yellow filled circles with orange border) or as a mixture of fcc and bcc phases (hollow orange circles). It is worth mentioning that in some papers a single bcc solid solution is reported (e.g. $Al_xCrFeNiCo$ ($x \geq 1.25$) in [48,54]) but in those cases dendritic microstructure evidences the presence of partitioning in two different phases [53] and the presence of a mixture of B2 ordered phase and bcc disordered phase is frequently reported [51,53]. Therefore, it can be clearly appreciated a boundary between single phase systems and multiphase systems around T_{eff} ~500 K. This value is reasonably comparable with room temperature. Moreover, experimental data show that research on HEAs is focused mainly on those alloys with the highest ΔS_{conf} (see the

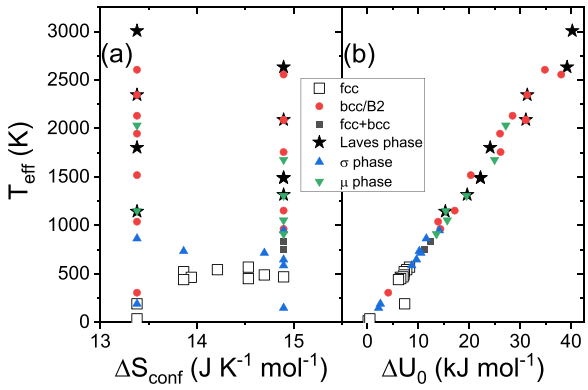

Fig. 6. T_{eff} for the quinary and sexinary alloys collected by Gorban et al. [15] grouped by their microstructures. In the case of intermetallic phases, bcc or fcc solid solutions may also appear.

experimental data covering the right extreme values in Fig. 5), which is not always the correct route when single phase solid solutions are the desired goal.

In order to test the model in a broader range of elements, the value of T_{eff} for the quinary and sexinary alloys collected by Gorban et al. [15] are shown in Fig. 6, distinguishing between those compositions leading to fcc solid solutions, bcc solid solutions, mixture of them or including intermetallic compounds (Laves, sigma, or mu phases). 16 elements (Al, Ti, V, Cr, Mn, Fe, Co, Ni, Cu, Zr, Nb, Mo, Hf, Ta, W, and Re) are combined in the 46 alloys shown. We found that fcc solid solutions appear below $T_{eff} \sim 600$ K (a limit roughly in agreement but above that found for AlCrCuFeCoNiCo system). Moreover, only three exceptions are found: two of them correspond to about 50% fcc plus 50% sigma phase (equiatomic quinary VCrFeCoNi and sexinary VCrFeCoNiCu), and ReMoWNbTa alloys with bcc structure. Concerning the former exceptions, intermetallic phases are not considered in the proposed model. Concerning the latter exception, it is interesting that B2 ordered structure can frequently appear in these systems to accommodate differences in the atomic radii and ReMoWNbTa shows a small 2% value of the parameter $\delta = 2.1\%$, well below the limit predicted by Yang et al. ($\delta < 6.6\%$) [14] to develop an ordered phase. Moreover, this limit was revised to be $\delta < 4\%$ [4,16]. The other alloys analyzed in our study and exhibiting bcc structures showed a higher value of $\delta > 4\%$ and an almost linear correlation can be found between this parameter and T_{eff} (see Supplementary content, figure 3S). Supplemental content also shows a comparison between the predicted and experimental lattice parameter for compositions with bcc and fcc structures (Fig. 4S).

Conclusions

A model to describe the stability of homogeneous solid solutions in high entropy alloys is developed from the potential parameters used to describe metallic bonding. The model assumes a first neighbor approach for solid solutions by averaging the potential coefficients over the contributions of the different atomic couples in the alloy. In the simple average model, the average potential coefficients can be obtained by simply averaging over the values of the corresponding elements.

The model is able to describe the deviations of the lattice parameter from the linear law due to Vegard. When potential coefficients are obtained averaging over the different couples of atoms, a good agreement with the experimental data can be obtained. Moreover, differences in the lattice parameter between ordered and disordered phases can be well reproduced.

Using the simple average model, a figure of merit is proposed as an effective temperature defined by the increment in the solid solution bonding energy over the mixture of pure phases divided by the configurational entropy ($T_{eff} = \Delta U_0 / \Delta S_{conf}$). In the particular case of the Al-Cr-Cu-Fe-Ni-Co system, a value of T_{eff} <500 K would lead to the formation of single phase solid solutions, whereas T_{eff} >500 K would lead to the partitioning of atoms in two or more different solid solutions.

Declaration of Competing Interest

The authors declare that they have no known competing financial interests or personal relationships that could have appeared to influence the work reported in this paper.

Acknowledgments

This work was supported by PAI of the Regional Government of Andalucía and the VII PPIT of University of Sevilla.

Supplementary materials

Supplementary material associated with this article can be found, in the online version, at doi:10.1016/j.mtla.2023.101744.

References

[1] A. Inoue, F.L. Kong, S.L. Zhu, A. Churyumov, W.J. Botta, Formation, structure and properties of pseudo-high entropy clustered bulk metallic glasses, J. Alloy. Compd. 820 (2020), 153164, https://doi.org/10.1016/j.jallcom.2019.153164.
[2] B. Cantor, I.T.H. Chang, P. Knight, A.J.B. Vincent, Microstructural development in equiatomic multicomponent alloys, Mater. Sci. Eng. A 375-377 (2004) 213–218, https://doi.org/10.1016/j.msea.2003.10.257.
[3] J.W. Yeh, S.K. Chen, S.J. Lin, J.Y. Gan, T.S. Chin, T.T. Shun, C.H. Tsau, S.Y. Chang, Nanostructured high-entropy alloys with multiple principal elements: novel alloy design concepts and outcomes, Adv. Eng. Mater. 6 (2004) 299, https://doi.org/10.1002/adem.200300567.
[4] Y. Zhang, T.T. Zhuo, Z. Tang, M.C. Gao, K.A. Dahmen, P.K. Liaw, Z.P. Lu, Microstructures and properties of high-entropy alloys, Prog. Mater. Sci. 61 (2014) 1–93, https://doi.org/10.1016/j.pmatsci.2013.10.001.
[5] D.B. Miracle, O.N. Senkov, A critical review of high entropy alloys and related concepts, Acta Mater. 122 (2017) 448–511, https://doi.org/10.1016/j.actamat.2016.08.081.
[6] M.C. Cao, D.B. Miracle, D. Maurice, X. Yan, Y. Zhang, J.A. Hawk, High-entropy functional materials, J. Mater. Res. 33 (2018) 3138–3155, https://doi.org/10.1557/jmr.2018.323.
[7] M. Widom, Modeling the structure and thermodynamics of high-entropy alloys, J. Mater. Res. 33 (2018) 2881–2898, https://doi.org/10.1557/jmr.2018.222.
[8] H.W. Luan, Y. Shao, J.F. Li, W.L. Mao, Z.D. Han, C. Shao, K.F. Yao, Phase stabilities of high entropy alloys, Scr. Mater. 179 (2020) 40–44, https://doi.org/10.1016/j.scriptamat.2019.12.041.
[9] Z.S. Nong, J.C. Zhu, Y. Cao, X.W. Yang, Z.H. Lai, Y. Liu, Stability and structure prediction of cubic phase in as cast high entropy alloys, Mater. Sci. Technol. 30 (2014) 363–368, https://doi.org/10.1179/1743284713Y.0000000368.
[10] H. Inui, K. Kishida, Z. Chen, Recent progress in our understanding of phase stability, atomic structures and mechanical and functional properties of high-entropy alloys, Mater. Trans. 63 (2022) 394–401, https://doi.org/10.2320/matertrans.MT-M2021234.
[11] G. Anand, R. Goodall, C.L. Freeman, Role of configurational entropy in body-centred cubic or face-centred cubic phase formation in high entropy alloys, Scr. Mater. 124 (2016) 90–94, https://doi.org/10.1016/j.scriptamat.2016.07.001.
[12] D.B. Miracle, High entropy alloys as a bold step forward in alloy development, Nat. Commun. 10 (2019) 1805, https://doi.org/10.1038/s41467-019-09700-1.
[13] E.J. Pickering, N.G. Jones, High-entropy alloys: a critical assessment of their founding principles and future prospects, Int. Mater. Rev. 61 (2016) 183, https://doi.org/10.1080/09506608.2016.1180020.
[14] X. Yang, Y. Zhang, Prediction of high-entropy stabilized solid-solutions in multi-component alloys, Mater. Chem. Phys. 132 (2012) 233–238, https://doi.org/10.1016/j.matchemphys.2011.11.021.
[15] V.F. Gorban, N.A. Krapivka, S.A. Firstov, Hihg-entropy alloys: interrelations between electron concentration, phase composition, lattice parameter, and properties, Phys. Met. Metall. 118 (2017) 970–981, https://doi.org/10.1134/S0031918X17080051.
[16] A.S. Rogachev, Structure, stability, and properties of high-entropy alloys, Phys. Met. Metallogr. 121 (2020) 733–764, https://doi.org/10.1134/S0031918X20080098.
[17] A.K. Singh, N. Kumar, A. Dwivedi, A. Subramaniam, A geometrical parameter for the formation of disordered solid solutions in multi-component alloys, Intermetallics 53 (2014) 112–119, https://doi.org/10.1016/j.intermet.2014.04.019.
[18] M.G. Poletti, L. Battezzati, Electronic and thermodynamic criteria for the occurrence of high entropy alloys in metallic systems, Acta Mater. 75 (2014) 297–306, https://doi.org/10.1016/j.actamat.2014.04.033.

[19] D.J.M. King, S.C. Middleburgh, A.G. McGregor, M.B. Cortie, Acta Mater. 104 (2016) 172–179, https://doi.org/10.1016/j.actamat.2015.11.040.
[20] W. Hume-Rothery, Lattice parameters of Solid Solutions in Silver, Nature (1935) 1038.
[21] A.R. Miedema, P.F. de Chatel, F.R. de Boer, Cohesion in alloys Fundamentals of a semi-empirical model, Phys. B 100 (1980) 1–28, https://doi.org/10.1016/0378-4363(80)90054-6.
[22] D.M. King, S.C. Middleburgh, L. Edwards, G.R. Lumpkin, M. Cortie, Predicting the crystal structure and phase transitions in high-entropy alloys, JOM 67 (2015) 2375–2380, https://doi.org/10.1007/S11837-015-1495-4.
[23] D.J.M. King, A.G. McGregor, Alloys Search and Predict (ASAP), 2015. https://www.AlloyASAP.com.
[24] Ashcroft, N.W.; Mermin, N.D., Solid State Physics, 1976, Brooks/Cole.
[25] C. Kittel, Introduction to Solid State Physics, 6th Ed., John Wiley & Sons, 1997.
[26] L. Battezatti, Solid solutions in metals: from hume-Rothery's rules to high entropy alloys, Acc. Sc. Torino Quaderni 30 (2019) 21–35.
[27] M. de Podesta, Understanding the Properties of Matter, 2nd Ed., Taylor and Francis, 2002.
[28] L. Pauling, Atomic radii and interatomic distances in metals, J. Am. Chem. Soc. 69 (1947) 542–553, https://doi.org/10.1021/ja01195a024.
[29] L. Vegard, Die konstitution der mischkristallen und die raumfüllung der atome, Z. Phys. 5 (1921) 17–26, https://doi.org/10.1007/BF01349680.
[30] J. Friedel, Deviations from Vegard's law 46 (1955) 514–516. 10.1080/14786440508520587.
[31] S.T. Murphy, A. Chroneos, C. Jiang, U. Schwingenschlögl, R.W. Grimes, Deviations from Vegard's law in ternary III-V alloys, Phys. Rev. B 82 (2010), 073201, https://doi.org/10.1103/PhysRevB.82.073201.
[32] C.Y. Fong, W. Weber, J.C. Phillips, Violation of Vegard's law in covalent semiconductor alloys, Phys. Rev. B 14 (1976) 5387, https://doi.org/10.1103/PhysRevB.14.5387.
[33] S. Datta Roy (Paul), S.K. Das, A green function estimation of correction to Vegard's law for isovalent substitutional defects in alkali halide crystals, Acta Phys. Pol. 97 (2000) 671–679, https://doi.org/10.12693/APhysPolA.97.671.
[34] T. Baidya, P. Bera, O. Kröcher, O. Safonova, P.M. Abdala, B. Gerke, R. Pöttgen, K. R. Priolkar, T.K. Mandal, Understanding the anomalous behavior of Vegard's law in Ce1−xMxO2 (M = Sn and Ti; $0 < x \leq 0.5$) solid solutions, Phys. Chem. Chem. Phys. 18 (2016) 13974–13983, https://doi.org/10.1039/C6CP01525E.
[35] M.N. Magomedov, On the deviation from the Vegard's law for the solid solutions, Solid State Commun. 322 (2020), 114060, https://doi.org/10.1016/j.ssc.2020.114060.
[36] V.A. Lubarda, On the effective lattice parameter of binary alloys, Mech. Mater. 35 (2003) 53–68, https://doi.org/10.1016/S0167-6636(02)00196-5.
[37] L. Zhang, S. Li, Empirical atom model of Vegard's law, Phys. B Condens. Matter 434 (2014) 38–43, https://doi.org/10.1016/j.physb.2013.10.066.
[38] H.W. King, Quantitative size-factors for metallic solid solutions, J. Mater. Sci. 1 (1966) 79–90, https://doi.org/10.1007/BF00549722.
[39] A.S.M. Handbook, Volume 3. Alloy Phase Diagrams, ASM International, 1992.
[40] A.M. Balagurov, I.A. Bobrikov, I. Golovin, Effects of ordering in Fe-xAl alloys, JETP Lett. 110 (2019) 585–591, https://doi.org/10.1134/S0021364019210057.
[41] R.W. Cahn, Lattice parameter changes on disordering intermetallics, Intermetallics 7 (1999) 1089–1094, https://doi.org/10.1016/S0966-9795(99)00035-7.
[42] T. Borkar, B. Gwalani, D. Choudhuri, C.V. Mikler, C.J. Yannetta, X. Chen, R. V. Ramanujan, M.J. Styles, M.A. Gibson, R. Banerjee, A combinatorial assessment of AlxCrCuFeNi2 ($0 < x < 1.5$) complex concentrated alloys: microstructure, microhardness, and magnetic properties, Acta Mater. 116 (2016) 63–76, https://doi.org/10.1016/j.actamat.2016.06.025.
[43] S. Uporova, V. Bykov, S. Pryanichnikov, A. Shubin, N. Uporova, Effect of synthesis route on structure and properties of AlCoCrFeNi high-entropy alloy, Intermetallics 83 (2017) 1–8, https://doi.org/10.1016/j.intermet.2016.12.003.
[44] K.B. Zhang, Z.Y. Fu, J.Y. Zhang, J. Shi, W.M. Wang, H. Wang, Y.C. Wang, Q. J. Zhang, Annealing on the structure and properties evolution of the CoCrFeNiCuAl high-entropy alloy, J. Alloy. Compd. 502 (2010) 295–299, https://doi.org/10.1016/j.jallcom.2009.11.104.
[45] S. Singh, N. Wanderka, K. Kiefer, K. Siemensmeyer, J. Banhart, Effect of decomposition of the Cr–Fe–Co rich phase of AlCoCrCuFeNi high entropy alloy on magnetic properties, Ultramicroscopy 111 (2011) 619–622, https://doi.org/10.1016/j.ultramic.2010.12.001.
[46] W. Wang, H. Li, P. Wei, W. Zhang, J. Chen, S. Yuan, Y. Fan, R. Wei, T. Zhang, T. Wang, C. Chen, F. Li, A corrosion-resistant soft-magnetic high entropy alloy, Mater. Lett. 304 (2021), 130571, https://doi.org/10.1016/j.matlet.2021.130571.
[47] P.F. Yu, L.J. Zhang, H. Cheng, H. Zhang, M.Z. Ma, Y.C. Li, G. Li, P.K. Liaw, R.P. Liu, The high-entropy alloys with high hardness and soft magnetic property prepared by mechanical alloying and high-pressure sintering, Intermetallics 70 (2016) 82–87, https://doi.org/10.1016/j.intermet.2015.11.005.
[48] M.S. Lucas, L. Mauger, J.A. Muñoz, Y. Xiao, A.O. Sheets, S.L. Semiatin, J. Horwath, Z. Turgut, Magnetic and vibrational properties of high-entropy alloys, J. Appl. Phys. 109 (2011) 07E307, https://doi.org/10.1063/1.3538936.
[49] B. Niu, F. Zhang, H. Ping, N. Li, J. Zhou, L. Lei, J. Xie, J. Zhang, W. Wang, Z. Fu, Sol-gel autocombustion synthesis of nanocrystalline high-entropy alloys, Sci. Rep. 7 (2017) 3421, https://doi.org/10.1038/s41598-017-03644-6.
[50] S. Guo, C. Ng, J. Lu, C.T. Liu, Effect of valence electron concentration on stability of fcc or bcc phase in high entropy alloys, J. Appl. Phys. 109 (2011), 103505, https://doi.org/10.1063/1.3587228.
[51] C.J. Tong, Y.L. Chen, J.W. Yeh, S.J. Lin, S.K. Chen, T.T. Shun, C.H. Tsau, S. Y. Chang, Microstructure characterization of Al x CoCrCuFeNi high-entropy alloy system with multiprincipal elements, Metall. Mater. Trans. A 36 (2005) 881–893, https://doi.org/10.1007/s11661-005-0283-0.
[52] Y. Zhang, Y.J. Zhou, J.P. Lin, G.L. Chen, P.K. Liaw, Solid-Solution Phase Formation Rules for Multi-component Alloys, Adv. Eng. Mater. 10 (2008) 534–538, https://doi.org/10.1002/adem.200700240.
[53] C. Li, J.C. Li, M. Zhao, Q. Jiang, Effect of alloying elements on microstructure and properties of multiprincipal elements high-entropy alloys, J. Alloy. Compd. 475 (2009) 752–757, https://doi.org/10.1016/j.jallcom.2008.07.124.
[54] H.P. Chou, Y.S. Chang, S.K. Chen, J.W. Yeh, Microstructure, thermophysical and electrical properties in AlxCoCrFeNi ($0 \leq x \leq 2$) high-entropy alloys, Mater. Sci. Eng. B 163 (2009) 184–189, https://doi.org/10.1016/j.mseb.2009.05.024.
[55] Y.J. Zhou, Y. Zhang, F.J. Wang, G.L. Chen, Phase transformation induced by lattice distortion in multiprincipal component CoCrFeNiCuxAl1−x solid-solution alloys, Appl. Phys. Lett. 92 (2008), 241917, https://doi.org/10.1063/1.2938690.
[56] J.W. Yeh, S.Y. Chang, Y.D. Hong, S.K. Chen, S.J. Lin, Anomalous decrease in X-ray diffraction intensities of Cu–Ni–Al–Co–Cr–Fe–Si alloy systems with multi-principal elements, Mater. Chem. Phys. 103 (2007) 41–46, https://doi.org/10.1016/j.matchemphys.2007.01.003.
[57] J.W. Yeh, S.J. Lin, T.S. Chin, J.Y. Gan, S.K. Chen, T.T. Shun, C.H. Tsau, S.Y. Chou, Formation of simple crystal structures in Cu-Co-Ni-Cr-Al-Fe-Ti-V alloys with multiprincipal metallic elements, Metall. Mater. Trans. A 35 (2004) 2533–2536, https://doi.org/10.1007/s11661-006-0234-4.
[58] L.H. Wen, H.C. Kou, J.S. Li, H. Chang, X.Y. Xue, L. Zhou, Effect of aging temperature on microstructure and properties of AlCoCrCuFeNi high-entropy alloy, Intermetallics 17 (2009) 266–269, https://doi.org/10.1016/j.intermet.2008.08.012.